Brazilian Journal
of Chemical
Engineering

ISSN 0104-6632
Printed in Brazil
www.abeq.org.br/bjche

Vol. 32, No. 02, pp. 489 - 500, April - June, 2015
dx.doi.org/10.1590/0104-6632.20150322s00003039

VAPOR-PHASE CATALYTIC CONVERSION OF ETHANOL INTO 1,3-BUTADIENE ON Cr-Ba/MCM-41 CATALYSTS

N. La-Salvia*, J. J. Lovón-Quintana and G. P. Valença

Laboratório para o Estudo de Processos de Adsorção e Catálise, LEPAC, Faculdade de Engenharia Química,
FEQ, Universidade Estadual de Campinas, UNICAMP, Cidade Universitária Zeferino Vaz,
Av. Albert Einstein 500, CEP: 13083-852, Campinas - SP, Brasil.
E-mail: nathalialasalvia@gmail.com

(Submitted: October 17, 2013 ; Revised: January 29, 2013 ; Accepted: March 30, 2014)

Abstract - Al-MCM-41, 16%Ba/Al-MCM-41 and 1.4%Cr-16%Ba/Al-MCM-41 were used as catalysts in the vapor-phase catalytic conversion of ethanol. Physical-chemical properties of the catalysts and the effect of barium and chromium on the Al-MCM-41 activity and 1,3-butadiene yield were studied. The catalysts were characterized by X-ray diffraction (XRD), N_2 physisorption (BET method), CO_2 chemisorption and Fourier transform infrared spectroscopy (FT-IR). When ethanol was completely converted on Al-MCM-41 and 16%Ba/Al-MCM-41, the reaction products showed a high selectivity for ethylene (90-98%). However, on the 1.4%Cr-16%Ba/Al-MCM-41 catalyst, a greater number of reaction products were obtained such as ethylene, acetaldehyde, diethyl ether and 1,3-butadiene. The maximum 1,3-butadiene yield obtained from ethanol reaction was 25% at 723 K and W/F_{EtOH} = 15 g h mol^{-1}. The latter result was obtained in a single step and without addition of reaction promoters (e.g., acetaldehyde, crotonaldehyde, hydrogen) in the feed stream to the reactor.
Keywords: MCM-41; Barium; Chromium; Ethanol reactions; 1,3-Butadiene.

INTRODUCTION

1,3-Butadiene (H_2C=CH-CH=CH_2) is a simple conjugated diene, a colorless gas at room temperature with a mild odor, and a non-corrosive but hazardous chemical due to its high volatility, flammability, reactivity, toxicity and carcinogenic properties [White, 2007; Levin *et al.*, 2004; Christian, 1996]. 1,3-Butadiene is an important chemical used as a monomer or co-monomer in the manufacturing of synthetic rubbers. For example, polybutadiene (PB), styrene–butadiene rubber (SBR) and nitrile-butadiene rubber (NBR) are widely used in tire products; thermoplastic resins such as acrylonitrile–butadiene–styrene (ABS) are used in automotive parts and business machines; and styrene-butadiene latex (SBL) is used in paints, paper coating, and carpet backings. 1,3-Butadiene is also an intermediate in the production of neoprene (polychloroprene) used in wetsuits, sleeves, orthopedic devices and electrical insulation and of adiponitrile, a precursor for the production of nylon 66 [White, 2007]. Commercially, 1,3-butadiene is obtained as a co-product from the steam cracking process of paraffinic hydrocarbons in petroleum refining to produce light olefins such as ethylene and propylene. Butadiene can also be produced by the catalytic dehydrogenation of n-butane and n-butene (Hourdry process) or by the oxidative dehydrogenation of n-butene (Oxo-D process) [Burla *et al.*, 2012].

Since 1,3-butadiene is a petrochemical product, developing alternative routes for its production from renewable resources have increased recently due to

*To whom correspondence should be addressed

environmental and economic issues. One alternative raw material is ethanol, considered to be one of the most relevant and well established renewable sources of carbon. Ethanol can be easily obtained from different feedstocks such as sucrose, starchy materials and lignocellulosic biomass. In the USA, ethanol is produced almost exclusively from corn, and in tropical and sub-tropical countries such as Brazil the most important source of biomass utilized for producing ethanol is sugar cane, either in the form of cane juice or cane molasses [Sánches, 2008; Cardona, 2007]. The US and Brazil are the largest suppliers of ethanol, and are responsible for 90% of the worldwide production [British Petroleum, 2011].

On the other hand, according Posada *et al.* (2013), there are twelve derivatives of commercial interest from ethanol. Five of these are categorized as favorable compounds to be produced compared to the petrochemical route (diethyl ether, 1,3-butadiene, ethyl acetate, propylene and ethylene), two as promising (acetaldehyde and ethylene oxide) and five as unfavorable derivatives (acetic acid, n-butanol, isobutylene, hydrogen and acetone) for an integrated biorefinery concept. Therefore, the search and the development of new routes for producing 1,3-butadiene from ethanol becomes viable.

In the last decades, several potentially useful catalysts have been proposed for the conversion of ethanol into 1,3-butadiene. The catalysts most often used in these reactions are mixed oxides with different dispersions and acid-base bifunctional properties. For example, direct synthesis of 1,3-butadiene from ethanol has been obtained using magnesia(basic)–silica(acidic) catalysts ($MgO(x)–SiO_2$, where x = Mg/Si) and other doped with transition metal oxides ($MO_x(y)/MgO_{(2)}–SiO_2$, where y = M/Si, and M = Cr, Mn, Fe, Co, Ni, Cu, Zn, Ag) [Makshina *et al.*, 2012]. According to Makshina *et al.* (2012), magnesia activates the aldol condensation reaction and favors the dehydrogenation, while silica catalyzes dehydration. The same authors suggested that the dispersion and crystallinity of the magnesia have little impact on the 1,3-butadiene yield, and the silica compositions of the catalysts could modify the 1,3-butadiene selectivity. Among other catalysts commonly used in these reaction are MgO/SiO_2 [Kvisle *et al.*, 1988], Al_2O_3:ZnO (60:40) [Bhattacharyya and Sanyal, 1967; Bhattacharyya and Avasthi, 1966], and ZrO_2/SiO_2 [Toussaint *et al.*, 1947]. Consequently, the synthesis of 1,3-butadiene from ethanol in one-step on acid-base bifunctional catalysts shows different and promising values of 1,3-butadiente yield. Thus, 2% was achieved on $2\%Ta_2O_5$-$98\%SiO_2$ [Jones *et al.*, 1945]; 14% on hydroxyapatite [Tsuchida *et al.*, 2008]; 16% on MgO/SiO_2 [Kvisle *et al.*, 1988]; 25% on $1\%Ag$-$10\%ZrO_2$-$500\%SiO_2$ [Jones *et al.*, 1945]; and 52, 56 and 58% on ZnO-MgO/SiO_2, Ag-MgO/SiO_2, and CuO-MgO/SiO_2, respectively [Makshina *et al.,* 2012]. The values above correspond to 1,3-butadiene yield from pure ethanol, without addition of reaction promoters (e.g., acetaldehyde, crotonaldehyde, hydrogen) in the feed stream to the reactor, commonly used to improve the 1,3-butadiene yield [Ordomskiy *et al.*, 2012; Jones *et al.*, 2011; Bhattacharyya and Sanyal, 1967; Bhattacharyya and Avasthi, 1966; Corson *et al.*, 1950].

Microporous molecular sieves with a pore diameter less than 2 nm are used as catalysts in many different reactions. However, reactions on these molecular sieves are diffusion limited. On the other hand, mesoporous molecular sieves with a pore diameter in the range from 2 to 10 nm have been used in acid-catalyzed reactions, particularly in the treatment of feedstock and the synthesis of large molecules for the production of fine chemical products [Beck *et al.*, 1992; Corma, 1997]. Consequently, the discovery of the mesoporous silica molecular sieve (MCM-41) by the Mobil Oil Company resulted in considerable attention because of its uniform structure and pore size distribution. However, the pure silica MCM-41 has a neutral framework [Corma, 1997; Herbst *et al*., 1995; Kresge *et al*., 1992], which limits its industrial application due to its poor hydrothermal stability, low catalytic activity and weak surface acidity [Li *et al.*, 2012; Sugiyama *et al.*, 2010; Tuel, 1999]. However, it is possible to modify the nature of the MCM-41 framework by incorporation of heteroelements. For example, when trivalent cations such as Al^{3+}, B^{3+}, Ga^{3+}, Fe^{3+} replace some of the silicon atoms in the walls of the mesoporous silica, the framework acquires a negative charge that can be compensated by protons, and the resulting solids can be used in acid catalysts [Tuel, 1999]. The Al-containing MCM-41 (Al-MCM-41) is one of the most studied MCM-41. Al-MCM-41 is formed by a hexagonal arrangement of parallel tubes with an ordered pore system of adjustable size in the range from 1.5 to >10 nm and a high surface area (≈ 1100 $m^2\ g^{-1}$) [Selvarej, 2003]. A very striking feature of this solid is the wide variety of synthetic methods used for its preparation, with a wide range of framework Si/Al ratios and the possibility of introducing various metals in the structural network, either by isomorphic substitution or post-synthesis impregnation [Corma, 1997].

Al-MCM-41 is an acid catalyst and, in order to favor the formation of 1,3-butadiene, basic sites are necessary. In this work we propose to obtain 1,3-

butadiene from ethanol on barium and chromium catalysts supported on Al-MCM-41. Chromium was chosen because of its known dehydrogenation properties. Barium was chosen for its alkaline properties. Barium catalysts supported on silica (2%BaO-98%SiO_2 and 10%BaO-90%SiO_2) have been previously studied for the production of 1,3-butadiene from ethanol, reaching less than 7% of 1,3-butadiene yield [Corson *et al*., 1950]. In addition, Kaya *et al.* (2010) were able to introduce barium in the pores of Al-MCM-41 without damaging the structure of the sieve. The chromium-barium-based catalysts supported on Al-MCM-41 are a new material, which sparked interest in studying them.

EXPERIMENTAL SECTION

Catalyst Preparation

Al-MCM-41 (15Si:1Al) was synthesized according to the procedure described elsewhere [Pires and Miranda, 2002]. Briefly, a solution with 630 cm^3 ammonium hydroxide (Merck, 25% PA) and 810 cm^3 of deonized water was prepared. To this mixture 6 g of hexadecyltrimethyl-ammonium bromide (Sigma Aldrich, 99%) and 1.5 g of aluminium sulfate-18-hydrate (Merck, 59%) were added. After solubilization, 30 cm^3 of tetraethyl orthosilicate (Sigma Aldrich, 98%) was added. The final solution was stirred at 420 rpm for 2 h, at room temperature. The material was filtered and dried overnight at 400 K. The sample was then calcined at 813 K for 11 h, the first 5 h in a nitrogen flow and the remaining time in a synthetic air flow. Finally, the resulting product was cooled to room temperature under continuous synthetic air flow and stored in a desiccator until use.

The Ba/Al-MCM-41 and Cr-Ba/Al-MCM-41 catalysts were prepared by introducing the metal ions (Ba^{+2} and Cr^{+3}) in the pores of the Al-MCM-41 by incipient wetness impregnation. Aqueous solutions of barium nitrate, $Ba(NO_3)_2$ (Sigma Aldrich, 99%) and chromium(III)-nitrate-nonahydrate, $Cr(NO_3)_3.9H_2O$ (Sigma Aldrich, 99%) were used to introduce the metallic ions. First, barium was introduced in the pores of Al-MCM-41. The weight percentage of barium was 16%. After impregnation of Al-MCM-41 with barium, the wet solids were dried at 400 K overnight. Subsequently, the solids were calcined in N_2 at 723 K for 5 h at a flow rate of 60 cm^3 min^{-1}. Then, the solids were cooled to room temperature in a N_2 flow and stored in a desiccator until use.

The chromium-barium-based catalysts supported on Al-MCM-41 were prepared by incipient wetness impregnation of the chromium precursor on the 16%Ba/Al-MCM-41 catalyst. The chromium concentration in the chromium-barium-based catalyst was 1.4% w/w. After impregnation with an aqueous chromium solution, the solids were dried at 400 K overnight and subsequently were calcined in a mixture of 5%H_2/N_2 at 723 K for 5 h at a total flow rate of 60 cm^3 min^{-1}. Then, the solids were cooled to room temperature in a N_2 flow (60 cm^3 min^{-1}). After reaching room temperature, the samples were kept in a N_2 flow for 30 min. Then, the sample was exposed to a mixture of 1%O_2/N_2 at a total flow rate of 60 cm^3 min^{-1} for 2 h. Finally, the samples were stored in a desiccator until use.

Catalyst Characterization

The bulk structure of the passivated solids was determined by the powder X-ray diffraction technique (XRD) using a Philips Model X'Pert diffractometer with Cu Kα1 radiation (λ = 0.154056 nm), with an intensity of 40 kV and current of 30 mA. The diffraction patterns were measured between 1.8º and 100º with a step size of 0.02º and a time step of 1 s. Prior to the XRD analysis, samples were dried at 393 K overnight and powdered. Identification of the diffraction peaks in the XRD patterns was done by comparing to JCPDS data.

The surface area of the solids was determined by N_2 adsorption at 77 K in a Micromeritics ASAP 2020 analyzer by the BET method [Brunauer *et al*., 1938]. Prior to analysis the samples (ca. 100 mg) were heated under vacuum from RT to 623 K at a rate of 10 K min^{-1}, and degassed at 623 K for 10 min. The total pore volume was measured by the amount of N_2 adsorbed at a relative pressure close to one (P/P_0 = 0.995). The average pore diameter was determined by Barrett-Joyner-Halenda (BJH) from the N_2 desorption isotherms.

The adsorption isotherms of CO_2 (White Martins, 99.999%) were measured at 310 K on a Micromeritics ASAP 2020 analyzer. The samples (ca. 80 mg) were degassed at 1×10^{-5} mmHg and 673 K for 2 h. The sample temperature was then decreased under vacuum to the analysis temperature and kept at this temperature for 10 min. In all analyses, two isotherms were obtained with equilibrium pressures between 50 and 250 mmHg. The second isotherm was obtained after degassing the sample for 30 min at 1×10^{-5} mmHg and the analysis temperature (310 K). The difference between the two isotherms and extrapolation to zero pressure was used as a measure of the amount of irreversibly adsorbed gas.

Fourier transform infrared spectroscopy (FT-IR)

was carried out on a Thermo Scientific (Nicolet 6700, Madison – USA) infrared spectrometer. Prior to analysis the samples were heated at 393 K overnight, finely milled and mixed with spectroscopic grade potassium bromide (KBr) in a ratio of ≈ 1:10. The powder was pressed up to 15 kg cm^{-2} for 10 min to form transparent pallets. The infrared radiation was allowed to pass through these transparent pallets and the measurements were obtained in the transmittance mode from 400 cm^{-1} to 4000 cm^{-1} with 64 scans and a resolution of 4 cm^{-1}.

In order to investigate the amount of coke deposited on the catalyst after ethanol reaction, thermogravimetric analysis (TGA) was carried out by using a TGA 2050 TA Instrument. The sample (ca. 10 mg) was placed in a platinum pan and exposed to a constant heating rate of 12 K/min from room temperatures to 973 K, under a synthetic air flow (10 mL/min).

Catalytic Testing

The catalytic tests were carried out in a U-shaped reactor made of Pyrex glass (6 mm ∅). The ethanol was fed into the reactor by a system composed of an evaporator and a saturator using as carrier N_2 gas at atmospheric pressure. Then, the reactor was installed in a tube furnace connected to a temperature programmer (EDGCON 5P, EDG Equipment). The gases used were N_2, (White Martins, Praxair INC, 99.999%) and H_2 (White Martins, Praxair INC, 99.995%). The gases were used as received with no further purification. The reaction products from the reactor were analyzed on a Hewlett-Packard 6890 gas chromatograph equipped with a C.G. 6095 Porapak Q column (2 m × 2 mm ∅, granulometry 80/100 mesh, Lot Nº 3001481707-10), with a thermal conductivity detector (TCD) and flame ionization detector (FID).

The mass of the catalysts was 30 mg. Prior to catalytic tests, the solids were pre-treated at 600 K in a 5%H_2/N_2 flow (60 cm^3 min^{-1}). After 1 h the H_2 flow was closed and only N_2 was flowed for 30 min. Then, using a bypass, the N_2 gas was conducted to the ethanol evaporator/saturator, and the saturation temperature of ethanol was adjusted to keep the W/F_{EtOH} ratio at 1.5, 15 and 150 g h mol^{-1}. Next, the ethanol reaction was started and the temperatures tested were 573, 623, 673, 723 and 773 K. The samples remained 2 h at each temperature, and three chromatographic analyses were obtained. Product selectivity was defined as: $PS(\%) = (Q_P/Q_{SP})\times100$, where Q_P is the number of moles of each product and Q_{SP} is the sum of the moles of the reaction products. The moles of solid products (such as small amount of coke) were not included. The product yield was defined as: $PY(\%) = (Q_P/Q_{EtOH})$, where Q_{EtOH} is the total number of moles of ethanol fed into the reactor.

RESULTS AND DISCUSSIONS

Characterization

The low-angle X-ray diffraction patterns of the mesoporous aluminosilicate molecular sieve Al-MCM-41 sample (Figure 1a) have up to three well-resolved peaks at 2Θ = 2.5°, 4.2°, and 4.9° corresponding to the crystalline planes (100), (110), and (200), respectively. The latter diffraction patterns suggests that the Al-MCM-41 samples prepared in this work have a hexagonal structure and ordered pore system with high porosity [Mingzhong *et al*., 2011; Beck *et al*.,1992].

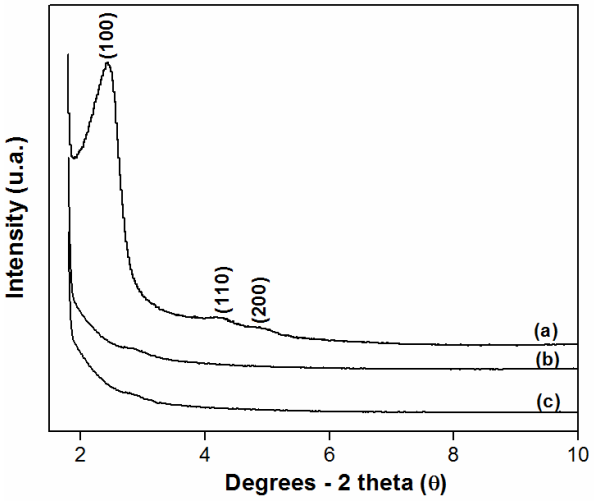

Figure 1: Low-angle XRD patterns of (**a**) Al-MCM-41, (**b**) 16%Ba/Al-MCM-41, (**c**) 1.4%Cr-16%Ba/Al-MCM-41.

After incorporation of the barium ions on Al-MCM-41 (16%Ba/Al-MCM-41) the charecteristic peak of the Al-MCM-41 hexagonal structure at 2Θ = 2.5° practically disappeared (Figure 1b), indicating a significant change of the structural properties of Al-MCM-41 due to formation of barium oxide species on the surface of the zeolite. Thus, on 16%Ba/MCM-41 samples barium orthosilicate (Ba_2SiO_4) was identified from the X-ray diffraction patterns (Figure 2b) at 2Θ = 27°, 29.6°, 30.4°, and 34° (PDF#77-0150) corresponding to crystalline planes (121), (112), (130), and (200), respectively. No other crystalline phases of barium were detected. After introduction

of chromium ions on the 16%Ba/MCM-41 samples (1.4%Cr-16%Ba/Al-MCM-41), the low-angle X-ray diffraction patterns of the samples (Figure 1c), were not different from that obtained for 16%Ba/MCM-41. However, the XRD diffraction lines corresponding to chromium species were very difficult distinguish (Figure 2c) because of the low content of chromium ions (≈ 1.4% w/w), indicating that chromium species are well dispersed over the surface of the solids. On the other hand, a very broad peak at about 2Θ = 18-30° observed in Figure 2a-c was attributed to amorphous SiO_2, which is formed during the heat-treatment steps.

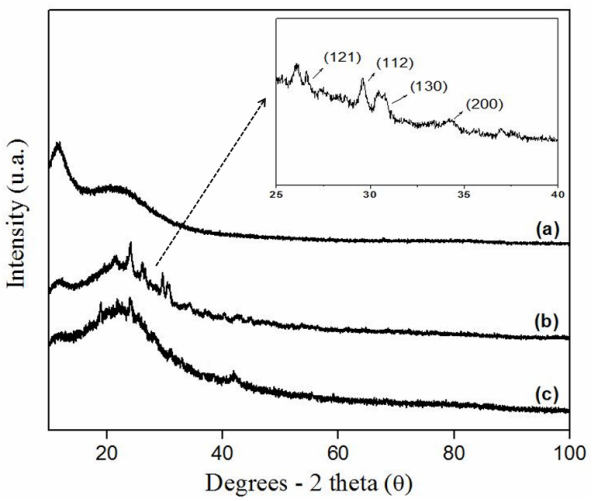

Figure 2: XRD patterns of (a) Al-MCM-41, (b) 16%Ba/Al-MCM-41, (c) 1.4%Cr-16%Ba/Al-MCM-41.

The N_2-adsorption-desorption isotherms are shown in Figure 3, and the surface properties of the catalysts measured by N_2 physisorption and CO_2 chemisorption are summarized in Table 1. The isotherms of the solids correspond to type IV (in the IUPAC classification), which is typical of mesoporous materials. The solids showed values of specific surface area between 460-1174 $m^2\ g^{-1}$ and the specific surface area of the catalysts decreased in the following order: Al-MCM-41 > 16%Ba/Al-MCM-41 > 1.4%Cr-16%Ba/Al-MCM-41. The surface area for the pure aluminosilicate is similar to those previously reported [Mingzhong *et al.*, 2011; Kaya *et al.*, 2010; Beck *et al.*, 1992]. However, it was observed that the addition of barium ions to the aluminosilicate caused a reduction of 40% in the surface area and ca. 15% in the total pore volume and pore diameter of Al-MCM-41. Furthermore, the addition of chromium ions to the 16%Ba/Al-MCM-41 showed a greater reduction in the surface area (60%), in the total pore volume (68%) and in the pore diameter (23%) of the pure aluminosilicate used as catalyst support. These latter results can be assigned to the formation of agglomerates of metal-oxide species blocking the entry of the channel structure of mesoporous Al-MCM-41.

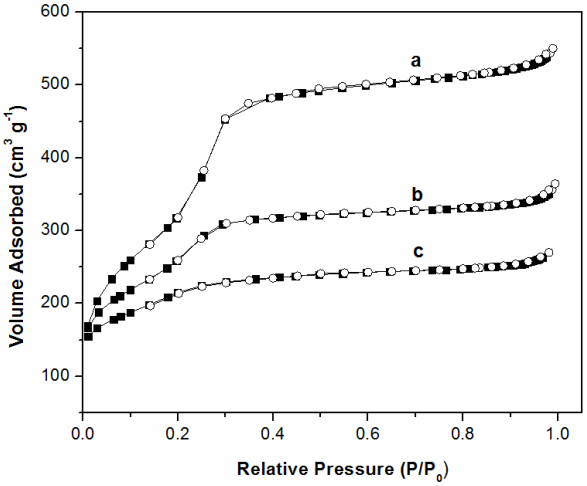

Figure 3: N_2 adsorption and desorption isotherms at 77 K. (a) Al-MCM-41, (b) 16%Ba/Al-MCM-41, (c) 1.4%Cr-16%Ba/Al-MCM-41. Filled squares = adsorption, open circles = desorption.

Regarding the measured CO_2 adsorption (Table 1), the CO_2 concentration per unit area increased with addition of barium and chromium in the following order: Al-MCM-41 < 16%Ba/Al-MCM-41 < 1.4%Cr-16%Ba/Al-MCM-41. In previous studies, it was reported that CO_2 can be absorbed irreversibly on OH^- groups (basic sites) producing CO_3^{2-} and H_2O species [Cheng *et al.*, 1998]. Therefore, an increase of the catalyst basicity can be assigned to the alkali-earth properties of barium [Yang and Kim, 2010; Zhang and Singh, 2008] and to the tendency to form carbonates on the chromium surfaces [Seiferth *et al.*, 1999; Kuhlenbeck *et al.*, 1992].

Table 1: Surface properties of the catalysts measured by N_2 physisorption and CO_2 chemisorption.

SOLIDS	Surface Area (BET, $m^2\ g^{-1}$)	Pore Volume ($cm^3\ g^{-1}$)	Pore Diameter (nm)	Density of Basic Sites ($\mu mol_{CO2}/m^2_{Al\text{-}MCM\text{-}41}$)
Al-MCM-41	1174	0.82	2.82	0.009
16%Ba/Al-MCM-41	695	0.42	2.44	0.024
1.4%Cr-16%Ba/Al-MCM-41	460	0.26	2.17	0.058

Figure 4 shows the IR transmission spectra of samples in the range 4000-400 cm^{-1}. Figure 4a presents the spectrum of Al-MCM-41 non-calcined samples in which the bands at 1489 cm^{-1} (CH_3), 2844 cm^{-1} (symmetric CH_2+CH_3) and 2916 cm^{-1} (asymmetric CH_2) can be assigned to the templating agent, hexadecyltrimethyl-ammonium bromide [Ryczkowsky *et al.*, 2005; Montes *et al.*, 1998]. Notwithstanding, after calcination of the Al-MCM-41 samples (Figure 4b), the bands at 1489, 2844 and 2916 cm^{-1} disappeared, indicating that the calcinations step used in this work was effective in removing the templating agent. The band around 800 cm^{-1} refers to the symmetrical Si-O-Si stretch. The deformation in the vibrational mode of O-Si-O is observed at 450 cm^{-1}. The broad band between 1000 and 1250 cm^{-1} was assigned to the asymmetric Si-O-Si stretch [Ryczkowsky *et al.*, 2005]. This band is composed of two bands, the main band at 1075 cm^{-1} and a smaller band at 1234 cm^{-1}. When the materials were calcined, the band at 1075 cm^{-1} moved toward a higher wavenumber [Ryczkowsky *et al.*, 2005; Zhao *et al.*, 1997]. Also, before and after calcination at 813 K Al-MCM-41 shows a wide band at 3450 cm^{-1} (Figure 4a,b), which was assigned to the stretching mode of adsorbed water [Kaya *et al.*, 2010]. Furthermore, after adding barium and chromium and heat-treatment at 723 K, no significant change was observed in the water band frequency.

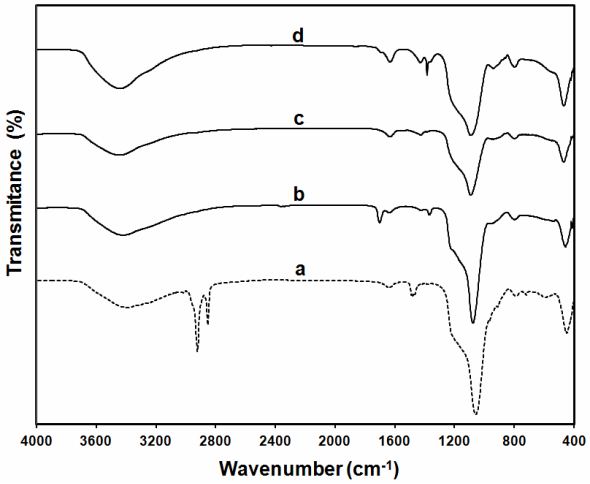

Figure 4: Infrared spectra of (a) Al-MCM-41 non-calcined, (b) Al-MCM-41 calcined, (c) 16%Ba/Al-MCM-41 calcined and (d) 1.4%Cr-16%Ba/Al-MCM-41 calcined.

Catalytic Tests

During the ethanol reaction experiments, diverse products and pathways of simultaneous reactions were observed, suggesting a great dependence on the reaction conditions and the nature of the surface of the solids. The experimental results of ethanol conversion / selectivity are shown in Figures 5 and 6 as a function of temperature (K) and as a function of W/F_{EtOH} (g h mol^{-1}).

The ethanol conversion (C_2H_5OH) on Al-MCM-41 was close to or greater than 99%, and three products were observed over the range temperature and W/F_{EtOH} tested (Figures. 5a, 6a). Al-MCM-41 showed high selectivity for ethylene (CH_2=CH_2), (> 98%), the rest being acetaldehyde (CH_3CHO) and propylene (C_2H_4=CH_2). This result is in agreement with the literature. According to Haishi *et al.* (2011), an Al-containing MCM-41 is highly active in the catalytic dehydration of lower alcohols to the corresponding olefins. However, ethylene from ethanol can be obtained by different reaction mechanisms (Eqs. (1)-(3)) [Haishi *et al.*, 2011; Makshina *et al.*, 2012; Sugiyama *et al.*, 2010]. Equation (1) seems to be the most favorable since, during ethanol conversion on Al-MCM-41, diethyl ether ($C_2H_5OC_2H_5$) was never observed. Acetaldehyde is typically formed by dehydrogenation reactions on basic sites (Eq. (4)) [Makshina *et al.*, 2012]. Thus, the low presence of acetaldehyde (< 1%) can be due to a low basic site concentration on Al-MCM-41 (Table 1). The presence of propylene is quite likely to be due to the high concentration of ethylene (> 98%). The mechanism of conversion of ethylene to propylene may involve the trimerization of ethylene to give hexane (C_5H_{10}=CH_2), followed by β-fission to produce propylene (Eq. (5)) [Murata *et al.*, 2008; Oikawa *et al.*, 2006].

$$C_2H_5OH \rightarrow CH_2 = CH_2 + H_2O \quad (1)$$

$$2\,C_2H_5OH \rightarrow C_2H_5OC_2H_5 + H_2O \quad (2)$$

$$C_2H_5OC_2H_5 \rightarrow 2\,CH_2 = CH_2 + H_2O \quad (3)$$

$$C_2H_5OH \rightarrow CH_3CHO + H_2 \quad (4)$$

$$3CH_2 = CH_2 \rightarrow C_5H_{10} = CH_2 \rightarrow 2C_2H_4 = CH_2 \quad (5)$$

The effect of reaction temperature and W/F_{EtOH} on the catalytic conversion of ethanol on the 16%Ba/Al-MCM-41 catalyst is shown in Figures 5b and 6b. In the ethanol reaction five compounds were observed over the range of temperatures and W/F_{EtOH} used in this work. Ethylene (CH_2=CH_2) and diethyl ether ($C_2H_5OC_2H_5$) were the major products; the sum of the selectivities for both products was 90±5%. The other three products, acetaldehyde (CH_3CHO), propylene (C_2H_4=CH_2) and ethane (C_2H_6), were found

in small amounts, the sum of their selectivities being in the range of 10±5%. The addition of barium resulted in an increase in the number of basic sites (ca. 2.5-fold), in agreement with results in the literature [Yang and Kim, 2010; Zhang and Singh, 2008], and in a 50% decrease of the surface area of Al-MCM-41 due to the formation of Ba_2SiO_4 particles that block the entry of the channel structure of the mesoporuos silica. At the beginning of the catalytic tests at 573 K and W/F_{EtOH} = 15 g h mol^{-1} (Figure 6b), the ethanol conversion was 66% and the selectivity for ethylene was 38% and for diethyl ether 56%. The ethanol conversion was ca. 100% when the temperature was 673 K at W/F_{EtOH} = 15 g h mol^{-1}. The selectivity for ethylene was increased up to ca. 90% at 673 K. The selectivity for diethyl ether fell to ca. 1% at 673 K. However, at low values of W/F_{EtOH} (1.5 g h mol^{-1}) and 723 K, the ethanol conversion was ca. 37% and similarly the selectivities for ethylene was 60% and for diethyl ether 24%. At high values of W/F_{EtOH} (> 15 g h mol^{-1}) and 723 K, the ethanol conversion reaches ca. 100% and the selectivity for ethylene was 90% and for diethyl ether 1%. These latter observations suggest that, at temperatures below 673 K, the formation of ethylene and diethyl ether takes place predominantly by Eqs. (2) and (3) and, above 673 K, the formation of ethylene may occur predominantly by means of Eq. (1).

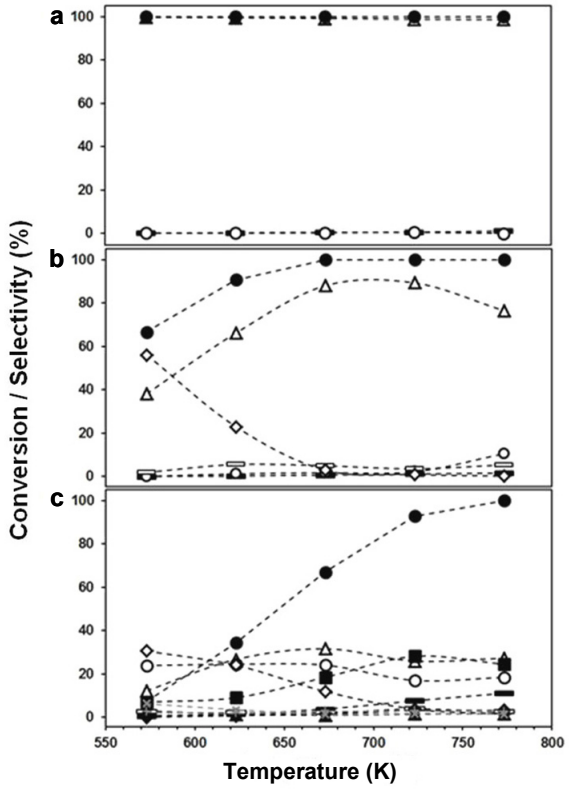

Figure 5: Ethanol conversion and selectivity as a function of temperature on (a) MCM-41, (b) 16%Ba/MCM-41 and (c) 1.4%Cr-16%Ba/Al-MCM-41. W/F_{EtOH} = 15 g h mol^{-1}. Filled circles = C_2H_5OH conversion and filled squares = CH_2=CHCH=CH_2, open circles = CH_3CHO, filled triangles = CH_3COCH_3, filled rhombus = CO_2, open rhombus = $C_2H_5OC_2H_5$, filled rectangles = C_2H_6, open triangles = CH_2=CH_2, filled rectangles = C_2H_4=CH_2, plus symbols = CH_3CH=CHCHO and multiplication symbols = C_4H_9OH.

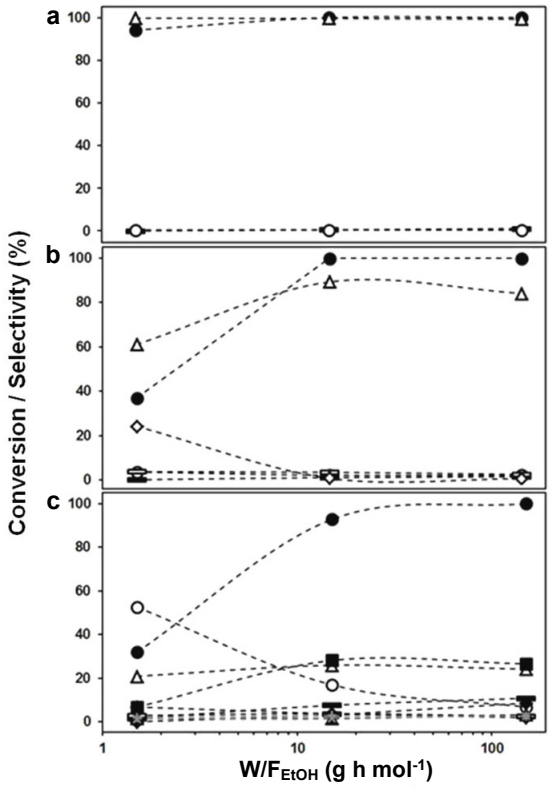

Figure 6: Ethanol conversion and selectivity as a function of W/F_{EtOH} (g h mol^{-1}) on (a) MCM-41, (b) 16%Ba/MCM-41 and (c) 1.4%Cr-16%Ba/Al-MCM-41. Reaction temperature = 723 K. Filled circles = C_2H_5OH conversion and filled squares = CH_2=CHCH=CH_2, open circles = CH_3CHO, filled triangles = CH_3COCH_3, filled rhombus = CO_2, open rhombus = $C_2H_5OC_2H_5$, filled rectangles = C_2H_6, open triangles = CH_2=CH_2, filled rectangles = C_2H_4=CH_2, plus symbols = CH_3CH=CHCHO and multiplication symbols = C_4H_9OH.

When the formation of acetaldehyde, propylene, and ethane on 16%Ba/Al-MCM-41 catalysts was compared with that obtained on Al-MCM-41, there was an increase in the acetaldehyde production by dehydrogenation reactions of ethanol (Eq. (4)) on 16% Ba/Al-MCM-41 catalysts. The propylene production remained the same (Eq. (5)), and ethane was produced (Figures 5a, 5b). The increase of acetaldehyde was due to the larger concentration of basic sites caused by the introduction of barium into the pores of Al-MCM-41. The propylene production was not affected by barium. Studies have shown that barium promotes the hydrogenation of light olefins [Wright and Weller, 1954]. Thus, the mechanism proposed in this work for ethane production comprises hydrogen production by dehydrogenation of ethanol (Eq. (4)), followed by the hydrogenation reaction of ethylene (Eq. (6)).

$$CH_2 = CH_2 + H_2 \rightarrow C_2H_6 \quad (6)$$

The ethanol reaction on 1.4%Cr-16%Ba/Al-MCM-41 catalyst as a function of reaction temperature and W/F_{EtOH} is shown in Figures 5c and 6c. The presence of chromium ions in the 1.4%Cr-16%Ba/Al-MCM-41 catalysts resulted in major structural changes and significant differences in the catalytic behavior in relation to 16%Ba/Al-MCM-41 catalysts. The chromium-containing solids showed a decrease in the specific surface area ca. 35% and a relative increase of 100% in the number of basic sites (Table 1) with respect to the 16%Ba/Al-MCM-41 catalysts. In the beginning of the catalytic tests, on 1.4%Cr-16%Ba/Al-MCM-41 at 573 K and W/F_{EtOH} = 15 g h mol^{-1}, the ethanol conversion was around 7%. However, with increasing temperature the ethanol conversion increased until it reached 100% at 773 K (Figure 5c). In all catalytic tests performed at 723 K on 1.4%Cr-16%Ba/Al-MCM-41, the ethanol conversion at W/F_{EtOH} = 1.5 g h mol^{-1} was nearly 30%; at W/F_{EtOH} = 15 g h mol^{-1} was ca. 90%; and at W/F_{EtOH} = 150 g h mol^{-1} was ca. 100% (Figure 6c). Ten compounds were formed in the reaction in the range of temperatures and W/F_{EtOH} studied. Four of these, ethylene (CH_2=CH_2), acetaldehyde (CH_3CHO), 1,3-butadiene (CH_2=CHCH=CH_2) and diethyl ether ($C_2H_5OC_2H_5$) were the major products, the sum of their selectivities being 80±6%. The other six products, namely propylene (C_2H_4=CH_2), ethane (C_2H_6), acetone (CH_3COCH_3), crotonaldehyde (CH_3CH=CHCHO), carbon dioxide (CO_2) and 1-butanol (C_4H_9OH), were found in smaller amounts, the sum of their selectivities being 17±6%.

The production of ethylene and diethyl ether in the chromium-barium-containing catalysts was 50% lower than that observed in solids containing only barium. However, the increase in the production of ethylene and decrease in the production of diethyl ether with reaction temperature were similar for both catalysts and can be explained by Eqs. (1)- (3). The production of acetaldehyde (Eq. (4)) was due to the higher concentration of basic sites on the chromium-barium-containing catalysts, which increased ca. 6-fold with respect to the catalysts containing only barium (Figure 5b, c). In addition, on 1.4%Cr-16%Ba/Al-MCM-41 catalysts there was a considerable production of 1,3-butadiene. The maximum selectivity of 28% was achieved at 723 K and W/F_{EtOH} = 15 g h mol^{-1} (Figure 5c). At 723 K the ethanol conversion was around 90%, corresponding to a yield of 1,3-butadiene of 25%. This last result is within the range of values of yield of 1,3-butadiene reported in the literature from ethanol in a single step, without addition of reaction promoters such as acetaldehyde, crotonaldehyde or hydrogen, commonly used for obtaining high selectivity for 1,3-butadiene [Ordomskiy *et al.*, 2012; Jones *et al.*, 2011; Tsuchida *et al.*, 2008; Kvisle *et al.*, 1988; Jones *et al.*, 1945]. Thus, the 1.4%Cr-16%Ba/Al-MCM-41 catalyst can be viewed as a new selective system for producing 1,3-butadiene from ethanol. However, the mechanism to obtain 1,3-butadiene from ethanol is complex and involves several reaction steps and the formation of intermediate products. One accepted reaction mechanism generally involves the following steps: formation of acetaldehyde by ethanol dehydrogenation (Eq. (4)); aldol condensation of acetaldehyde and dehydration to crotonaldehyde (Eq. (7)); Meerwein-Ponndorf-Verley reaction between ethanol and crotonaldehyde to obtain crotyl alcohol (CH_3CH=$CHCH_2OH$) and acetaldehyde (Eq. (8)); and dehydration of crotyl alcohol to obtain 1,3-butadiene (Eq. (9)) [Makshina, 2012; Jones, 2011; Kvisle, 1988; Toussaint, 1947; Jones, 1949]. Nevertheless, to obtain the true kinetic behavior for this complex system of reactions it is necessary to conduct further studies involving the identification and monitoring of intermediate species of the reaction by analytical techniques *in situ*.

$$2CH_3CHO \rightarrow CH_3CH = CHCHO + H_2O \quad (7)$$

$$CH_3CH = CHCHO + C_2H_5OH \rightarrow CH_3CH = CHCH_2OH + CH_3CHO \quad (8)$$

$$CH_3CH = CHCH_2OH \rightarrow CH_2 = CHCH = CH_2 + H_2O \quad (9)$$

The selectivities of conversion to propylene and

ethane on the 1.4%Cr-16%Ba/Al-MCM-41 catalyst were close to those observed in the solids containing only barium (Eqs. (5), (6)) and were not significantly affected by chromium (Figures 5c, 6c). However, on chromium-containing catalysts other compounds such as crotonaldehyde, acetone, carbon dioxide, and 1-butanol were produced. Regardless of the reaction conditions, the selectivity for each compound was less than 3%. According to the reaction mechanisms proposed in the literature, it is generally accepted that ethanol is first dehydrogenated to acetaldehyde, which then undergoes an aldol condensation with ethanol forming acetaldol. Acetaldol is then dehydrated to produce cis/trans butane (Eq. (7)) [Jones, 2011]. Acetone is produced by aldol condensation of acetaldehyde. The reaction of aldol with lattice oxygen $O_{(S)}$ on the catalyst follows to give the surface intermediate. Then, dehydrogenation and decarboxylation of the intermediate give acetone. (Eq. (10)) [Nishiguchi *et al.,* 2005; Elliott and Pennella, 1989]. Carbon dioxide can be obtained as a byproduct of acetone production (Eq. (10)) or by steam reforming of ethanol (Eq. (11)). 1-Butanol is obtained via a reaction network and involves formation of various intermediates adsorbed on the catalyst surface [Tsuchida *et al.*, 2008; Tsuchida *et al.*, 2006]. However, 1-butanol production can be described by the overall reaction, Eq. (12).

$$2CH_3CHO + O_{(s)} \rightarrow CH_3COCH_3 + CO_2 + H_2 \quad (10)$$

$$C_2H_5OH + 3H_2O \rightarrow 2CO_2 + 6H_2 \quad (11)$$

$$2C_2H_5OH \rightarrow C_4H_9OH + H_2O \quad (12)$$

In order to evaluate the performance of the 1.4%Cr-16%Ba/Al-MCM-41 catalyst, an ethanol reaction test was performed for 24 h in the optimal reaction conditions obtained in this work (Figure 7). In the first minutes of reaction a conversion of ethanol of ca. 100% was obtained with a 1,3-butadiene selectivity close to 30%. During the first 10 h of reaction, the ethanol conversion dropped to 80%, and the selectivity for 1,3-butadiene remained constant around 28% (yield ≈ 25 ± 3%). In the following 14 h of reaction, the conversion of ethanol dropped to 65%, while the selectivity for 1,3-butadiene went down to 20% (yield ≈ 13%). The selectivity for acetaldehyde (19.7%) and ethylene (15.5%) remained constant throughout the reaction. The main reason for the catalyst deactivation may be due to the gradual deposition of coke on the catalyst surface as a result of decomposition of hydrocarbons, with reaction by-products strongly adsorbed on the active sites. The formation of coke is probably associated with kinetic restrictions which hindering carbon gasification. The latter can be verified by TGA (Figure 8) after ethanol reaction on the 1.4%Cr-16%Ba/Al-MCM-41 catalyst. The TGA profile in the temperature range from 675 to 875 K shows a broad peak corresponding to removal of coke deposited on the catalyst surface (ca. 9.7% w/w).

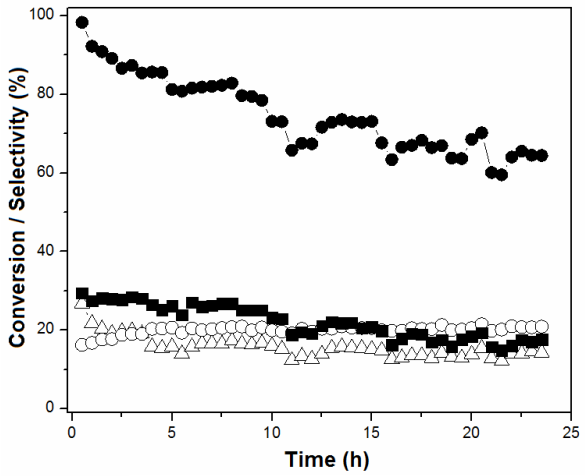

Figure 7: Ethanol conversion and selectivity as a function of time on 1.4%Cr-16%Ba/Al-MCM-41. Reaction temperature = 723 K and W/F_{EtOH} = 15 g h mol^{-1}. Filled circles = C_2H_5OH conversion and filled squares = CH_2=CHCH=CH_2, open circles = CH_3CHO and open triangles = CH_2=CH_2.

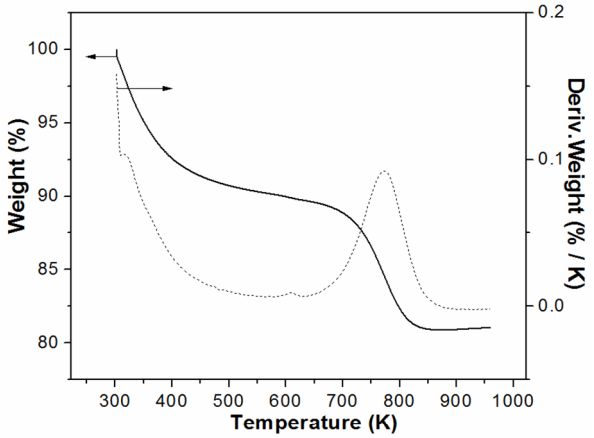

Figure 8: TGA curves of 1.4%Cr-16%Ba/Al-MCM-41 after ethanol reaction at 723 K and W/F_{EtOH} = 15 g h mol^{-1}.

CONCLUSIONS

In this study, Al-MCM-41, 16%Ba/Al-MCM-41, and 1.4%Cr-16%Ba/Al-MCM-41 were used as cata-

lysts for the vapor-phase catalytic conversion of ethanol. At the temperatures and W/F_{EtOH} used in this work, light hydrocarbons and oxygenated compounds with carbon numbers in the range from C1 to C4 were produced, the overall amount increasing in the following order: Al-MCM-41 < 16%Ba/Al-MCM-41 < 1.4%Cr-16%Ba/Al-MCM-41. These results were associated with changes in the structure of the solids upon successive introduction of the barium and chromium ions on Al-MCM-41, which results in an increase in the concentration of basic sites. Nevertheless, 1,3-butadiene was only observed on the 1.4%Cr-16%Ba/Al-MCM-41 catalysts, obtained from ethanol with a maximum yield of 25% at 723 K and W/F_{EtOH} = 15 g h mol^{-1}.

ACKNOWLEDGMENTS

This research was supported by the Brazilian funding support agency: CNPq. We are grateful for the financial support. The authors would also like to thank Matthew Maylath for reviewing the manuscript for its English usage.

NOMENCLATURE

ABS	Acrylonitrile-Butadiene-Styrene
BET	Brunauer- Emmett-Teller method
BJH	Barrett-Joyner- Halenda method
FID	Flame Ionization Detector
FTIR	Fourier Transform Infrared Spectroscopy
NBR	Nitrile-Butadiene Rubber
Oxo-D	Oxidative Dehydrogenation
PB	Polybutadiene
PS	Product Selectivity
PY	Product Yield
Q_{EtOH}	Total quantity (moles) of ethanol fed into the reactor
Q_P	Number of moles of each product
Q_{SP}	Sum of moles of the reaction products
SBL	Styrene-butadiene latex
SBR	Styrene-butadiene rubber
TCD	Thermal Conductivity Detector
TGA	Thermogravimetric Analysis
XRD	X-ray diffraction

REFERENCES

Beck, J. S., Vartuli, J. C., Roth, J. W., Leonowicz, M. E., Kresge, C. T., Schmitt, K. D., Chu, C. T. W., Olson, O. H., Sheppard, E. W., Mccullen, S. B., Higgins, J. B., Schlenkert, J. L., A new family of mesoporous molecular sieves prepared with liquid crystal templates. J. Am. Chem. Soc., 27, p. 10834-10843 (1992).

Bhattacharyya, S. K., Avasthi, B. N., J., One-step catalytic conversion of ethanol to butadiene in fluidized bed. Appl. Chem., 16, p. 239-244 (1966).

Bhattacharyya, S. K., Sanyal, S. K., Kinetic study on the mechanism of the catalytic conversion of ethanol to butadiene. J. Catal., 7, p. 152-158 (1967).

British Petroleum, BP Energy Outlook 2030. London, United Kingdom (2011).

Brunauer, S., Emmett, P. H., Teller, E., Adsorption of gases in multimolecular layers. J. Am. Chem. Soc., 60, p. 309-319 (1938).

Burla, J., Fehnel, R., Louie, P., Terpeluk, P., Two-step production of 1.3-butadiene from ethanol. Scholarly Commons, University of Pennsylvania, Philadelphia (2012).

Cardona, C. A., Sánchez, O. J., Fuel ethanol production: Process design trends and integration opportunities. Bioresour. Technol., 98, p. 2415-2457 (2007).

Cheng, Z. H., Yasukawa, A., Kandori, K., Ishikawa, T., FTIR Study of Adsorption of CO_2 on nonstoichiometric calcium hydroxyapatite. Langmuir 14, p. 6681-6686 (1998).

Christian, M. S., Review of reproductive and developmental toxicity of 1.3- butadiene. Toxicology, 113, p. 137-143 (1996).

Corma, A., From microporous to mesoporous molecular sieve materials and their use in catalysis. Chem. Rev., 97, p. 2373-2419 (1997).

Corson, B. B., Jones, H. E., Welling, C. E., Hinckley, J. A., Stahly, E. E., Butadiene from ethyl alcohol. Industrial and Engineering Chemistry, 42, 2, p. 359-373 (1950).

Elliot, D. J., Pennella, F., The formation of ketones in the presence of carbon monoxide over $CuO/ZnO/A1_2O_3$. J. Catal., 119, p. 359-367 (1989).

Haishi, T., Kasai, K., Iwamoto, M., Fast and quantitative dehydration of lower alcohols to corresponding olefins on mesoporous silica catalyst. Chem. Lett., 40, p. 614-616 (2011).

Herbst, J. A., Kresge, C. T., Olson, D. H., Schmitt, K. D., Vartuli, J. C., Wang, D. C. I., US Patent 5,378, p. 440 (1995).

Jones, H. E., Stahly, E. E., Corson, B. B., Butadiene from ethanol. Reaction mechanism J. Am. Chem. Soc., 71, p. 1822-1828 (1949).

Jones, M. D., Keir, C. G., Iulio, C. D., Robertson, R. A. M., Williams, C. V., Apperley, D. C., Investigations into the conversion of ethanol into 1.3-butadiene. Catal. Sci. Tech., 1, p. 267-272 (2011).

Kaya, E., Oktar, N., Karakas, G., Urtezão, K. T., Synthesis and characterization of Ba/MCM-41. J. Chem., 34, p. 935-943 (2010).

Kresge, C. T., Leonowicz, M. E., Roth, W. J., Vartuli, J. C., Beck, J. S., Ordered mesoporous molecular sieves synthesized by a liquid-crystal template mechanism. Nature, 359, p. 710-712 (1992).

Kuhlenbeck, H., Xu, C., Dillmann, B., Habel, M., Adam, B., Ehrlich, D., Wohrab, S., Freund, H. J., Adsorption and reaction on oxide surfaces: CO and CO_2 on Cr_2O_3. Ber. Bunsenges. Phys. Chem., 96, p. 15-27 (1992).

Kvisle, S., Aguero, A., Sneeden, R. P. A., Transformation of ethanol into 1.3-butadiene over magnesium oxide/silica catalysts. Appl. Catal., 43, p. 117-131 (1988).

Levin, M. E., Hill, A. D., Zimmerman, L. W., Paxson, T. E., The reactivity of 1.3- butadiene with butadiene-derived popcorn polymer. Hazard J. Mater., 115, p. 71-90 (2004).

Li, B., Wu, K., Yuan, T., Han, C., Xu, J., Pang, X., Synthesis, characterization and catalytic performance of high iron content mesoporous Fe-MCM-41. Microporous and Mesoporous Materials, 151, p. 277-281 (2012).

Makshina, E. V., Janssens, W., Sels, B. F., Jacobs, P. A., Catalytic study of the conversion ethanol into 1.3-butadiene. Catal. Today, 198, p. 338-344 (2012).

Mingzhong, C., Wenyan, H., Ronghua, H., MCM-41 – Supported bidentate phosphine rhodium complex: An efficient and recyclable heterogeneous catalyst for the hydrosilylation of olefins. Chin. J. Chem., 29, 1629-1634 (2011).

Montes, A., Cosenza, E., Giannetto, G., Urquieta, E., Melo, R. A., Gnep, N. S., Guisnet, M., Thermal decomposition of surfactant occluded in mesoporous MCM-41 type solids. Mesoporous Molec. Siev., 117, p. 237-242 (1998).

Murata, K., Inaba, M., Takahara, I., Effects of surface modifications of H-ZSZ-5 catalysts on direct transformation of ethanol into lower olefins. J. J. Pet. Inst., 51, p. 234-239 (2008).

Nishiguchi, T., Matsumoto, T., Kanai, H., Utani, K., Matsumura, Y., Shen, W., Imamura, S., Catalytic steam reforming of ethanol to produce hydrogen and acetone. Appl. Catal., A, 279, p. 273-277 (2005).

Oikawa, H., Shibata, Y., Inazu, K., Iwase, Y., Murai, K., Hyodo, S., Kobayashi, G., Baba, T., Highly selective conversion of ethene to propene over SAPO-34 as a solid acid catalyst. Appl. Catal., A, 312, p. 181-185 (2006).

Ordomskiy, V. V., Sushkevich, V. L., Ivanova, I. I., Patent WO 2012/015340 A1 (2012).

Pires, E. L., Miranda, E. A., Gas-phase enzymatic esterification on immobilized lypases in MCM-41 molecular sieves. Chem. Biol. Interact., 963, p. 98-100 (2002).

Posada, J. A., Patel, A. D., Roes, A., Blok, K., Faaij, A. P., Patel, M. K., Potential of bioethanol as a chemical buiding block for biorefineries. Bioresour. Technol., 132, p. 490-499 (2013).

Ryczkowski, J., Goworek, J., Gac, W., Pasieczna, S., Borowiecki, T., Temperature removal of templating agent from MCM-41 silica materials. Thermochim. Acta, 434, p. 02-08 (2005).

Sánchez, O. J., Cardona, C. A., Trends in biotechnological production of fuel ethanol from different feedstocks. Bioresour. Technol., 99, p. 5270-5295 (2008).

Seiferth, O., Wolter, K. B., Dillmann, B., Klivenyi, G., Freund, H.-J., Scarano, D., Zecchina, A., IR investigations of CO_2 adsorption on chromia surfaces: Cr_2O_3(0001)/Cr(110) versus polycrystalline α-Cr_2O_3. Surf. Sci., 421, p. 176-190 (1999).

Selvarej, M., Pandurangan, A., Seshadri, K. S., Synthesis, characterization and catalytic application of MCM-41 mesoporous molecular sieves containing Zn and Al. Appl. Catal., A, 242, p. 347 (2003).

Sugiyama, S., Kato, Y., Wada, T., Ogawa, S., Nakagawa, K., Sotowa, K., Ethanol conversion on MCM-41 and FSM-16, and ON Ni-Doped MCM-41 and FSM-16 prepared without hydrothermal conditions. Top. Catal., 53, p. 550-554 (2010).

Toussaint, W. J., Dunn, J. T., Jackson, D. R., Production of butadiene from alcohol. Ind. Eng. Chem., 39, p. 120-125 (1947).

Tsuchida, T., Kubo, J., Yoshioka, T., Sakuma, S., Takeguchi, T., Ueda, W., Reaction of ethanol over hydroxyapatite affected by Ca/P ratio of catalyst. J. Catal., 259, p. 183-189 (2008).

Tsuchida, T., Yoshioka, T., Sakuma, S., Takeguchi, T., Ueda, W., Direct synthesis of n-butanol from ethanol over nonstoichiometric hydroxyapatite. Ind. Eng. Chem. Res., 45, p. 8634-8642 (2006).

Tuel, A., Modification of mesoporous silicas by incorporation of heteroelements in the framework. Microporous Mesoporous Mater., 27, p. 151-169 (1999).

White, W. C., Butadiene production process overview. Chem. Biol. Interact., 166, p. 10-14 (2007).

Wright, L., Weller, S., The catalytic activity of barium and calcium hydrides. II. The nature of the catalyst. J. Am. Chem. Soc., 76, p. 5305 (1954).

Yang, S., Kim, J., Ahn, W., CO_2 adsorption over ion-exchanged zeolite beta with alkali and alkaline earth metal ions. Microporous Mesoporous Mater.,

165, p. 90-94 (2010).

Zhang, J., Singh, R., Webley, P. A., Alkali and alkaline-earth cation exchanged chabazite zeolites for adsorption based CO_2 capture. Microporous Mesoporous Mater., 111, p. 478-487 (2008).

Zhao, X. S., Lu, G. Q., Whittaker, A. K., Millar, G. J., Zhu, H. Y., Comprehensive study of surface chemistry of MCM-41 using 29Si CP/MAS, NMR, FTIR, pyridine-TPD and TGA. J. Phys. Chem., B, 101, p. 6525-6531 (1997).